Structure
Article

The Differential Regulation of p38α by the Neuronal Kinase Interaction Motif Protein Tyrosine Phosphatases, a Detailed Molecular Study

Dana May Francis,[1,4] Ganesan Senthil Kumar,[1,4] Dorothy Koveal,[2] Antoni Tortajada,[2] Rebecca Page,[2] and Wolfgang Peti[1,3,*]
[1]Department of Molecular Pharmacology, Physiology and Biotechnology
[2]Department of Molecular Biology, Cell Biology and Biochemistry
[3]Department of Chemistry
Brown University, Providence, RI 02912, USA
[4]These authors contributed equally to this work
*Correspondence: wolfgang_peti@brown.edu
http://dx.doi.org/10.1016/j.str.2013.07.003

SUMMARY

The MAP kinase p38α is essential for neuronal signaling. To better understand the molecular regulation of p38α we used atomistic and molecular techniques to determine the structural basis of p38α regulation by the two neuronal tyrosine phosphatases, PTPSL/PTPBR7 (PTPRR) and STEP (PTPN5). We show that, despite the fact that PTPSL and STEP belong to the same family of regulatory proteins, they interact with p38α differently and their distinct molecular interactions explain their different catalytic activities. Although the interaction of PTPSL with p38α is similar to that of the previously described p38α:HePTP (PTPN7) complex, STEP binds and regulates p38α in an unexpected manner. Using NMR and small-angle X-ray scattering data, we generated a model of the p38α:STEP complex and define molecular differences between its resting and active states. Together, these results provide insights into molecular regulation of p38α by key regulatory proteins.

INTRODUCTION

The mitogen-activated protein kinases (MAPKs) p38, ERK, and JNK are central to evolutionarily conserved signaling pathways that are present in all eukaryotic cells. Each MAPK cascade is activated in response to a diverse array of extracellular signals and culminates in the dual phosphorylation of a threonine and a tyrosine residue in the MAPK activation loop (Dérijard et al., 1995). Dually phosphorylated MAPKs then phosphorylate both cytosolic and nuclear targets, with the localization and duration of MAPK activity determining the cellular response to the initial extracellular signal. MAPK signal duration is finely controlled by multiple phosphatases, including three kinase interaction motif protein tyrosine phosphatases (KIM-PTPs): PTPSL/PTPBR7 (PTPRR), STEP (PTPN5), HePTP (PTPN7 and LC-PTP) (Hendriks et al., 1995; Lombroso et al., 1991; Zanke et al., 1992). KIM-PTPs control MAPK signaling by two mechanisms: (1) the KIM-PTP binds to an unphosphorylated MAPK to sequester it in the cytosol (known as the resting-state complex); and (2) the KIM-PTP dephosphorylates and inactivates a phosphorylated MAPK (known as the active-state complex) (Tárrega et al., 2002; Xu et al., 2009).

Increasing evidence suggests a crucial role for MAPK signaling in the central nervous system (CNS), and aberrant phosphorylation within the CNS is associated with a multitude of neurological disorders, including Alzheimer's disease and Parkinson's disease (Kim and Choi, 2010). Correspondingly, an additional layer of MAPK regulation is present within neurons. Two KIM-PTPs, PTPSL and STEP, are expressed within discrete regions of the CNS. PTPSL expression is highest in the cerebellum, while STEP is expressed in the hippocampus, striatum, amygdale, and cortex (Chirivi et al., 2004; Lombroso et al., 1993; Van Den Maagdenberg et al., 1999).

PTPSL, STEP, and the other KIM-PTP, HePTP, have a 17-residue kinase interaction motif (KIM or D-motif) that is essential for their interaction with ERK2 and p38 (Blanco-Aparicio et al., 1999; Saxena et al., 1999). The KIM binds to a conserved binding site that is formed by the hydrophobic docking groove and an acidic patch named the common docking (CD) site (together known as the KIM binding site or D-motif recruitment site) (Tárrega et al., 2002; Zhou et al., 2006). The KIM sequence is well conserved across the KIM-PTP family. All three KIMs contain basic residues, proposed to engage the CD site, upstream of a hydrophobic motif (L-X-L-X-Φ, where Φ is a methionine in STEP and PTPSL and a valine in HePTP; Figure 1A). Previously, we used nuclear magnetic resonance (NMR) spectroscopy and isothermal titration calorimetry (ITC) to define the interface of $HePTP_{KIM}$ binding to p38α. We determined that the hydrophobic motif occupies three hydrophobic pockets within the p38α hydrophobic docking groove, while its basic residues interact with the acidic patch (Francis et al., 2011a).

C terminal to the KIM is a region known as the kinase-specificity sequence (KIS), which is followed by a globular PTP catalytic domain (CAT) (Eswaran et al., 2006; Muñoz et al., 2003; Mustelin et al., 2005). Whereas the CAT is essential for dephosphorylation of the MAPK by the KIM-PTP, the importance of the KIS remains ambiguous, especially because the KIS sequence is divergent among the KIM-PTP family members. We previously

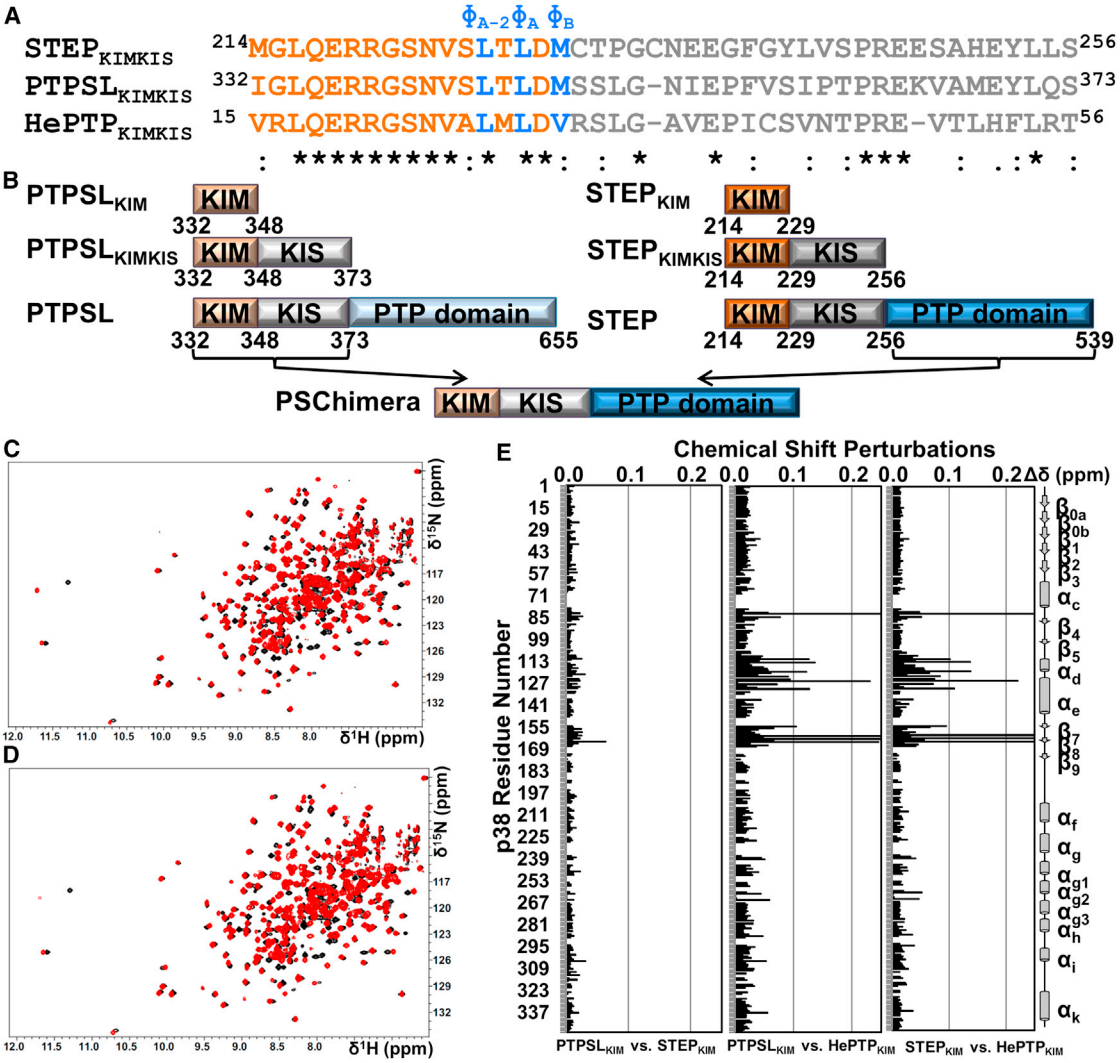

Figure 1. The Mode of KIM Binding Is Conserved within the KIM-PTP Family

(A) Sequences of $STEP_{KIMKIS}$, $PTPSL_{KIMKIS}$, and $HePTP_{KIMKIS}$ and conservation as determined using ClustalW (Larkin et al., 2007). KIM residues are colored in orange and blue. KIS residues are colored in gray.

(B) Constructs used in this study.

(C) 2D [^{1}H,^{15}N] TROSY spectrum of [^{2}H,^{15}N]-p38α (black) overlaid with the 2D [^{1}H,^{15}N] TROSY spectrum of [^{2}H,^{15}N]-p38α:$PTPSL_{KIM}$ (red; 1:8 molar ratio p38α:$PTPSL_{KIM}$).

(D) 2D [^{1}H,^{15}N] TROSY spectrum of [^{2}H,^{15}N]-p38α (black) overlaid with the 2D [^{1}H,^{15}N] TROSY spectrum of [^{2}H,^{15}N]-p38α:$STEP_{KIM}$ (red; 1:8 molar ratio p38α:$STEP_{KIM}$).

(E) Histograms show the combined ^{1}H/^{15}N CSPs versus p38α residue for the final titration points of each $KIM\text{-}PTP_{KIM}$ peptide with [^{2}H,^{15}N]-p38α.

See also Figure S1.

showed that the $HePTP_{KIS}$ is highly flexible and contributes significantly to the interaction between HePTP and p38α, while $HePTP_{CAT}$ does not interact with unphosphorylated p38α. This was corroborated by small-angle X-ray scattering (SAXS) experiments that showed that the p38α:HePTP resting-state complex is elongated in solution (Francis et al., 2011a). Whether the extensive KIS interaction, limited CAT interaction, and extended resting-state conformation observed in p38α:HePTP are common features of all p38α:KIM-PTP resting-state complexes is currently unknown.

Similar studies with a different MAPK, ERK2, revealed that the ERK2:HePTP resting-state complex shares several of these features. As with p38α, $HePTP_{CAT}$ does not interact with ERK2 in the resting state, and the ERK2:HePTP resting-state complex is extended in solution (Piserchio et al., 2012). However, phosphorylation of ERK2 leads to a domain rearrangement in which $HePTP_{CAT}$ rotates by nearly 180°, the ERK2:HePTP complex compacts, and the HePTP catalytic site residue moves by ~65 Å to allow for dephosphorylation of ERK2 (Francis et al., 2011b). The flexibility of the $HePTP_{KIS}$ and the absence of an interaction between ERK2 and $HePTP_{CAT}$ are critical to facilitate this large rearrangement.

Here, we combined NMR spectroscopy, SAXS, ITC experiments, and HADDOCK modeling to delineate the interaction of

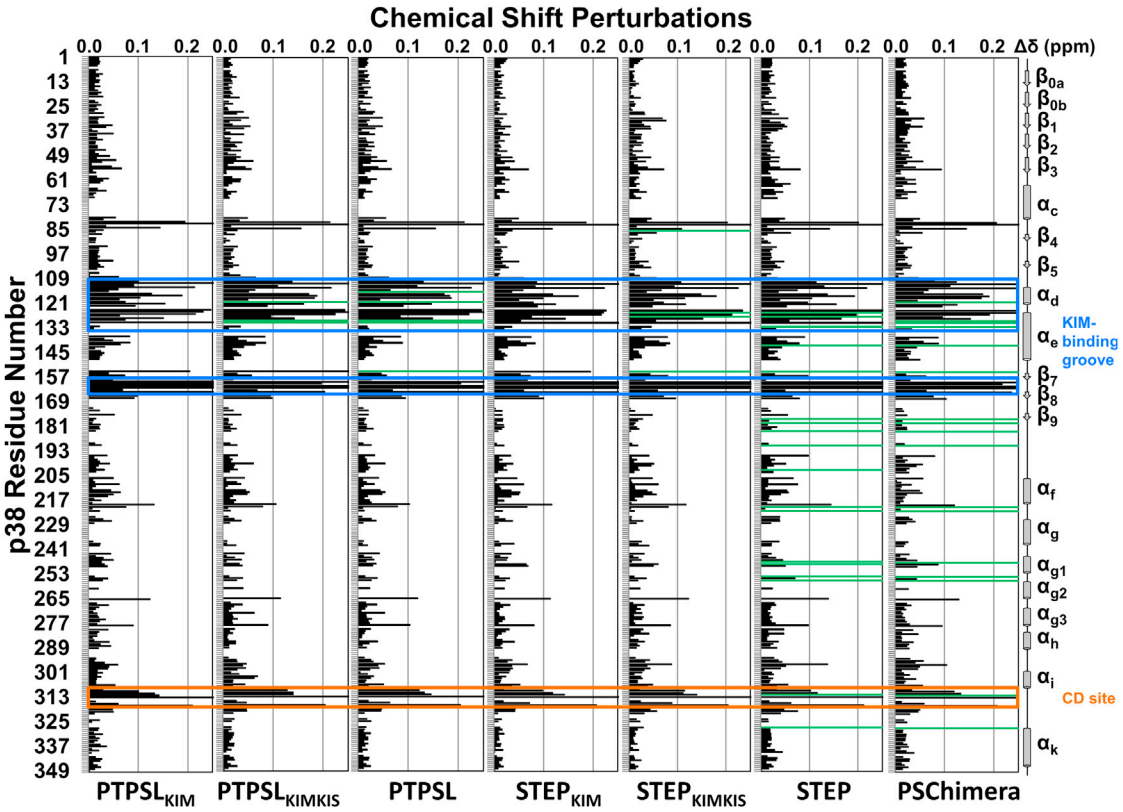

Figure 2. PTPSL and STEP Interaction with p38α

Histograms showing the combined $^{1}H/^{15}N$ CSP versus p38α residue for the following experiments: p38α with $PTPSL_{KIM}$ (1:8 molar ratio), $PTPSL_{KIMKIS}$ (1:3 molar ratio), PTPSL (1:1 ratio; SEC purified), $STEP_{KIM}$ (1:8 molar ratio), $STEP_{KIMKIS}$ (1:8 molar ratio), STEP (1:1 ratio; SEC purified), and PSChimera (1:1 ratio; SEC purified). Residues that form the p38α hydrophobic docking groove and the CD site are highlighted by blue and orange boxes, respectively. Residues with peak line widths broadened beyond detection upon titration are colored in green. See also Figure S3.

p38α with STEP and PTPSL. In combination with experiments conducted with HePTP, these studies serve as a detailed atomic-level characterization of MAPK regulation by an entire family of regulators—the KIM-PTP family. Our results reveal key differences between the interactions of p38α with each KIM-PTP. We show that the interaction of p38α with PTPSL is closely related to the interaction of HePTP, whereas the interaction of p38α with STEP is quite different and includes an unexpected contribution from $STEP_{CAT}$.

RESULTS

KIM Binding to p38α Is Conserved within the KIM-PTP Family

We used NMR spectroscopy to define the p38α binding interface of the $STEP_{KIM}$ and $PTPSL_{KIM}$ peptides (constructs used in this study are illustrated in Figure 1B). Each peptide was individually titrated into [^{2}H,^{15}N]-p38α until binding was saturated (1:1, 1:3, 1:5, 1:8 molar ratio of p38α:peptide) and two-dimensional (2D) [^{1}H,^{15}N] TROSY spectra were recorded (Figures 1C and 1D; Figure S1A available online). The fully saturated 2D [^{1}H,^{15}N] TROSY spectra of p38α:$PTPSL_{KIM}$ and p38α:$STEP_{KIM}$ (100 μM [^{2}H,^{15}N]-p38α:800 μM peptide) are highly similar (Figure 1E; Figure S1B). All peak shifts are in fast exchange and can be readily followed with the exception of three peaks that map to the MAPK-specific insert (L262–Q264) and are broadened beyond detection independent of ligand (Figure S1A). As expected, both peptides caused significant chemical shift perturbations (CSPs) for residues located in the KIM binding site, including helix αD, helix αE, the αD–αE loop, the β7–β8 turn, loop 4, and the CD site (Figure 2). Thus, like $HePTP_{KIM}$, $PTPSL_{KIM}$ and $STEP_{KIM}$ engage all three hydrophobic pockets and interact with the acidic patch, demonstrating that the mode of KIM binding to p38α is conserved within the KIM-PTP family.

However, there are small differences among the CSPs induced by $STEP_{KIM}$ and $PTPSL_{KIM}$. L164 in β8 exhibits the largest CSP difference among the 2D [^{1}H,^{15}N] TROSY spectra of p38α:$PTPSL_{KIM}$ and p38α:$STEP_{KIM}$ (Figure 1E; Figure S1B). The N-terminal residues of the KIM (Ile in $PTPSL_{KIM}$; Met in $STEP_{KIM}$) are the only residues not identical between the two peptides; therefore, any differences between the two spectra are a result of the differential interaction of this residue with p38α. Based on the structure of ERK2:$HePTP_{KIM}$, this residue is immediately adjacent to the β7–β8 turn, further supporting our NMR results (Zhou et al., 2006).

Although the KIM binding mode is conserved among the KIM-PTPs, the $HePTP_{KIM}$ sequence is only ~75% conserved when compared with $PTPSL_{KIM}$ and $STEP_{KIM}$ (Figure 1A). This leads

Table 1. Thermodynamic and Dissociation Constants for p38α:KIM-PTP Domains Derived from ITC Experiments at 25°C

Interaction	K_d (nM)	ΔH (kcal·mol^{-1})	TΔS (kcal·mol^{-1})	ΔG (kcal·mol^{-1})
p38α: $STEP_{KIM}$	3,567 ± 208	−37.7 ± 2.5	−30.2 ± 2.5	−7.4 ± 0.1
p38α: $STEP_{KIMKIS}$	1,340 ± 135	−34.7 ± 1.4	−26.6 ± 1.5	−8.0 ± 0.1
p38α: STEP	577 ± 71	−28.8 ± 2.0	−20.3 ± 2.0	−8.5 ± 0.1
p38α: $STEP_{F274A/F281A}$	1,074 ± 105	−24.2 ± 0.4	−16.0 ± 0.4	−8.2 ± 0.1
p38α: $STEP_{F281A/I307A}$	1,062 ± 36	−34.3 ± 1.1	−26.2 ± 1.0	−8.2 ± 0.1
p38α: $STEP_{M285A/I307A}$	592 ± 106	−27.6 ± 0.5	−19 ± 0.3	−8.5 ± 0.1
p38α: $PTPSL_{KIM}$	2,840 ± 135	−33.0 ± 1.7	−25.4 ± 1.7	−7.6 ± 0.1
p38α: $PTPSL_{KIMKIS}$	1,527 ± 23	−38.8 ± 6.1	−30.8 ± 6.1	−7.9 ± 0.1
p38α: PTPSL	382 ± 65	−30.2 ± 1.5	−21.4 ± 1.4	−8.8 ± 0.1
p38α: PSChimera	309 ± 4	−27.2 ± 0.7	−18.3 ± 0.7	−8.9 ± 0.0

See also Figure S2.

to changes in the chemical environment for residues within the p38α KIM binding site, which are readily observed in the 2D [^{1}H,^{15}N] TROSY spectra (Figure S1C). $PTPSL_{KIM}$ and $STEP_{KIM}$ perturb nine more peaks than $HePTP_{KIM}$ (Francis et al., 2011a). Compared to $HePTP_{KIM}$, $PTPSL_{KIM}$ and $STEP_{KIM}$ interact differentially with several residues within the hydrophobic binding groove and loop 4, including N82, A111, L113, C119, L122, D124, D125, V127, L130, S154, E160, C162, and L164 (Figure 1E). These NMR CSP experiments correspond well with ITC measurements that showed $PTPSL_{KIM}$ and $STEP_{KIM}$ bind p38α approximately two times tighter than does $HePTP_{KIM}$ (Table 1; Figure S2).

An NMR View of the Interaction between PTPSL and p38α

We expanded the NMR experiments to define the binding interface of PTPSL with p38α. In this experiment, [^{2}H,^{15}N]-p38α was incubated with unlabeled PTPSL, the 78 kDa p38α:PTPSL complex was purified by size exclusion chromatography (SEC), and a 2D [^{1}H,^{15}N] TROSY spectrum was immediately recorded (Figure S3C).

Direct comparison of the 2D [^{1}H,^{15}N] TROSY spectra of free and PTPSL-bound p38α reveals CSPs of 41 peaks, 36 in fast exchange and 5 peaks with line widths broadened beyond detection (N115, Q120, F129, L130, and S154; Figure 2). Like $PTPSL_{KIM}$, PTPSL perturbed residues clustered within the hydrophobic binding groove and the acidic patch of p38α (Figure 2). Two peaks, N115 (line widths broadened beyond detection) and V127, are perturbed by full-length PTPSL but not by $PTPSL_{KIM}$, with additional peaks experiencing larger CSPs (G110, D112, I116, K118, Q120, and Q310) (Figure 2). Correspondingly, full-length PTPSL binds approximately seven times tighter to p38α than does $PTPSL_{KIM}$ (Table 1; Figure S2).

The majority of the additional CSPs map to a region of p38α that interacts with $HePTP_{KIS}$ (Francis et al., 2011a). Although the $PTPSL_{KIS}$ and $HePTP_{KIS}$ sequences are only ~50% conserved, this region of p38α is thus also likely interacting with $PTPSL_{KIS}$. To determine whether a peptide composed of the $PTPSL_{KIM}$ and $PTPSL_{KIS}$ sequences (i.e., $PTPSL_{KIMKIS}$) can recapitulate the binding of full-length PTPSL to p38α, we titrated the $PTPSL_{KIMKIS}$ into [^{2}H,^{15}N]-p38α, and a series of 2D [^{1}H,^{15}N] TROSY spectra were recorded (Figure S3B). Titration of a three-fold molar excess of the $PTPSL_{KIMKIS}$ peptide (100 μM [^{2}H,^{15}N]-p38α:300 μM $PTPSL_{KIMKIS}$) resulted in a nearly identical 2D [^{1}H,^{15}N] TROSY spectrum as that of p38α:PTPSL (Figure 2, Figure S3H). Differences include residues N115 and S154, which are broadened beyond detection by full-length PTPSL but are either not perturbed (N115) or undergo a large CSP (S154) with $PTPSL_{KIMKIS}$, respectively (Figure S3H). Furthermore, a direct comparison of the 2D [^{1}H,^{15}N] TROSY spectra of p38α:$PTPSL_{KIM}$ with p38α:$PTPSL_{KIMKIS}$ shows larger CSPs for four residues (M109, K118, E160, and L164), and three peaks (Q120, F129, and L130) are broadened beyond detection by $PTPSL_{KIMKIS}$ but not by $PTPSL_{KIM}$ (Figure S3H). Consistent with these results, the $PTPSL_{KIMKIS}$ binds p38α approximately two times tighter than does $PTPSL_{KIM}$ (Table 1; Figure S2).

The p38α:PTPSL Resting-State Complex Is Extended in Solution

The interactions of $PTPSL_{KIM}$, $PTPSL_{KIMKIS}$, and PTPSL with p38α are highly similar. PTPSL perturbed few residues outside of the KIM binding site, confirming that the KIM is the essential anchor for the interaction of PTPSL with p38α. Indeed, we used NMR spectroscopy to probe the interaction of p38α with $PTPSL_{CAT}$, a construct lacking residues 332–360, which includes the KIM; no interactions between p38α and isolated $PTPSL_{CAT}$ were detected (Figures S4A and S4C). This is consistent with previous results from NMR experiments that showed that the isolated $HePTP_{CAT}$ did not interact with either p38α or ERK2 (Francis et al., 2011a; Piserchio et al., 2012).

Consequently, we used SAXS to determine the size and shape of the p38α:PTPSL resting-state complex. The p38α:PTPSL complex was purified by SEC, and SAXS data were recorded at Beamline X9A at the National Synchrotron Light Source (Brookhaven National Laboratories). Using the Guinier approximation of five independent SAXS samples, a radius of gyration (R_g) of 33.1 ± 0.5 Å was calculated for the p38α:PTPSL complex (Table 2; Figure 3A). A maximum particle dimension (D_{max}) of 105 Å was determined by analysis of the *P*(r) function (Table 2; Figures 3D and 3E). These values for R_g and D_{max} are highly similar to those determined for the p38α:HePTP and ERK2:HePTP resting-state complexes and demonstrate that, under resting conditions, p38α and PTPSL adopt an extended conformation, with a rather

Table 2. SAXS Analysis of p38α:PTPSL, p38α:STEP, and pp38α:STEP Complexes

	p38:PTPSL	p38:STEP (Resting)	pp38:STEP (Active)
Guinier approximation			
R_g (Å)	33.1 ± 0.5	29.9 ± 0.3	28.5 ± 0.3
P(r) function calculation			
Q range ($Å^{-1}$)	0.013–0.303	0.013–0.304	0.014–0.297
R_g (Å)	34.1	29.8	28.2
D_{max} (Å)	105	95	80
Structure modeling			
χ	1.4 ± 0.1	1.9 ± 0.2	1.0 ± 0.1
NSD	1.30 ± 0.04	1.09 ± 0.03	1.00 ± 0.03

limited interaction surface, consistent with the NMR CSP experiments.

The p38α:STEP Resting-State Complex Is Compact

An equivalent SAXS measurement was performed for the p38α:STEP resting-state complex. The Guinier approximation of four independent SAXS samples was used to calculate an R_g of 29.9 ± 0.3 Å, showing that the R_g of the p38α:STEP resting-state complex is ~3.0 Å smaller than that of the p38α:PTPSL and p38α:HePTP resting-state complexes (Table 2; Figure 3B). To analyze this difference in more detail, we determined the molecular envelope of the p38α:STEP resting-state complex (Table 2; Figures 3D and 3F). A D_{max} of 95 Å was determined by analysis of the *P*(r) function, which is ~10–15 Å shorter than the p38α:PTPSL and p38α:HePTP complexes (Table 2; Figure 3D). Thus, the p38α:STEP resting-state complex is more compact than both the p38α:KIM-PTP and the ERK2:HePTP resting-state complexes. Therefore, unlike PTPSL and HePTP, which have limited interaction surfaces with p38α, this result suggested that STEP may interact more extensively with p38α.

STEP Has Interactions with p38α Outside of the KIM Binding Pocket

To test this hypothesis, we performed NMR CSP experiments with full-length STEP and [^{2}H,^{15}N]-p38α. Here, [^{2}H,^{15}N]-p38α was incubated with unlabeled STEP, the 78 kDa p38α:STEP complex purified by SEC, and a 2D [^{1}H,^{15}N] TROSY spectrum recorded (Figure S3F). Direct comparison of the 2D [^{1}H,^{15}N] TROSY spectra of free and STEP-bound p38α reveals CSPs of 58 peaks, 40 in fast exchange and 18 with peak line widths that are broadened beyond detection (Figure 2). As expected, like $STEP_{KIM}$, STEP perturbs residues in the p38α KIM binding site (Figure 2). Surprisingly, STEP perturbed significantly more residues in p38α than did $STEP_{KIM}$ and caused several additional peaks to broaden beyond detection, decreasing the total number of peaks in the 2D [^{1}H,^{15}N] TROSY spectrum of STEP-bound p38α (Figure 2). Direct comparison of the 2D [^{1}H,^{15}N] TROSY spectra of p38α:$STEP_{KIM}$ and p38α:STEP reveals three additional residues (V30, M109, and L164) with CSPs and 18 additional peaks (D125, V127, Y132, I141, S154, D177, M179, V183, A190, Q202, R220, L222, L247, K248, S254, R256, H312, and E328) that are broadened beyond detection by full-length STEP (Figure S3I). Correspondingly, full-length STEP binds approximately six times tighter to p38α than does $STEP_{KIM}$ (Table 1; Figure S2). Mapping the additional perturbations reveals a previously undetected p38α interaction surface (herein referred to as the PTP site), which connects the p38α activation loop to the MAPK-specific insert.

To corroborate our findings, we used a divide and conquer approach. To determine whether the $STEP_{KIS}$ accounts for this additional interaction, a peptide composed of the $STEP_{KIMKIS}$ sequence was titrated into [^{2}H,^{15}N]-p38α, and a series of 2D [^{1}H,^{15}N] TROSY spectra was recorded (Figure S3E). Interestingly, the p38α:$STEP_{KIMKIS}$ spectrum (100 μM [^{2}H,^{15}N]-p38α:800 μM $STEP_{KIMKIS}$) is similar to that of p38α:$STEP_{KIM}$ at the same molar ratio (Figure 2; Figure S3I). Direct comparison of the 2D [^{1}H,^{15}N] TROSY spectra of p38α:$STEP_{KIM}$ and p38α:$STEP_{KIMKIS}$ reveals differences in seven residues: V30, M109, and E160 show CSPs, while G85, D125, V127, and S154 are broadened beyond detection (Figure S3I). Using ITC, we determined that $STEP_{KIMKIS}$ binds approximately two and a half times tighter than does $STEP_{KIM}$ but two times weaker than full-length STEP does (Table 1; Figure S2). Importantly, the $STEP_{KIMKIS}$ did not affect residues within the PTP site (Figure 2). This suggests that the additional changes in the NMR spectrum must be the result of an interaction between the STEP catalytic domain ($STEP_{CAT}$) and p38α.

p38α:PSChimera Complex

To confirm that $STEP_{CAT}$ interacts directly with p38α, we generated a chimeric protein in which $PTPSL_{KIMKIS}$ was fused with $STEP_{CAT}$ (herein referred to as the PSChimera; Figure 1B). The PSChimera was expressed, purified, and incubated with [^{2}H,^{15}N]-p38α. The p38α:PSChimera complex was then purified by SEC, and a 2D [^{1}H,^{15}N] TROSY spectrum of the complex was recorded (Figure S3G).

Within and around the p38α KIM binding site, the PSChimera affected the p38α 2D [^{1}H,^{15}N] TROSY spectrum in a PTPSL-like manner (Figure 2). Notably, additional changes in the p38α 2D [^{1}H,^{15}N] TROSY spectrum, which correspond to peaks that define the PTP site, were also identified (Figure 2). Thus, the PSChimera, which has a $PTPSL_{KIMKIS}$ and a $STEP_{CAT}$ domain, interacts in a PTPSL-like manner with its KIMKIS and in a STEP-like manner at the PTP site. Minor differences between the interaction of the PSChimera and STEP with p38α at the PTP site include Q202 and K248, which are not broadened beyond detection with PSChimera (K248 does experience a small CSP). Similar to STEP, 17 peaks in the PTP site broaden beyond detection with PSChimera, demonstrating that the $STEP_{CAT}$ interaction with p38α is independent of the KIMKIS sequence. Furthermore, NMR interaction studies showed that titration of unlabeled, isolated $STEP_{CAT}$ (lacking residues 214–243 including the KIM) with [^{2}H,^{15}N]-p38α results in nonspecific interactions throughout the p38α surface—further reinforcing the critical importance of KIM anchoring for p38α regulation (Figures S4B and S4C). The chimeric protein has a slightly higher binding affinity than does PTPSL or STEP for p38α (Table 1). This binding affinity is the product of the $PTPSL_{KIM}$, which binds the tightest of the three KIM-PTP_{KIM} peptides, coupled with the additional binding strength afforded by the $STEP_{CAT}$ interaction.

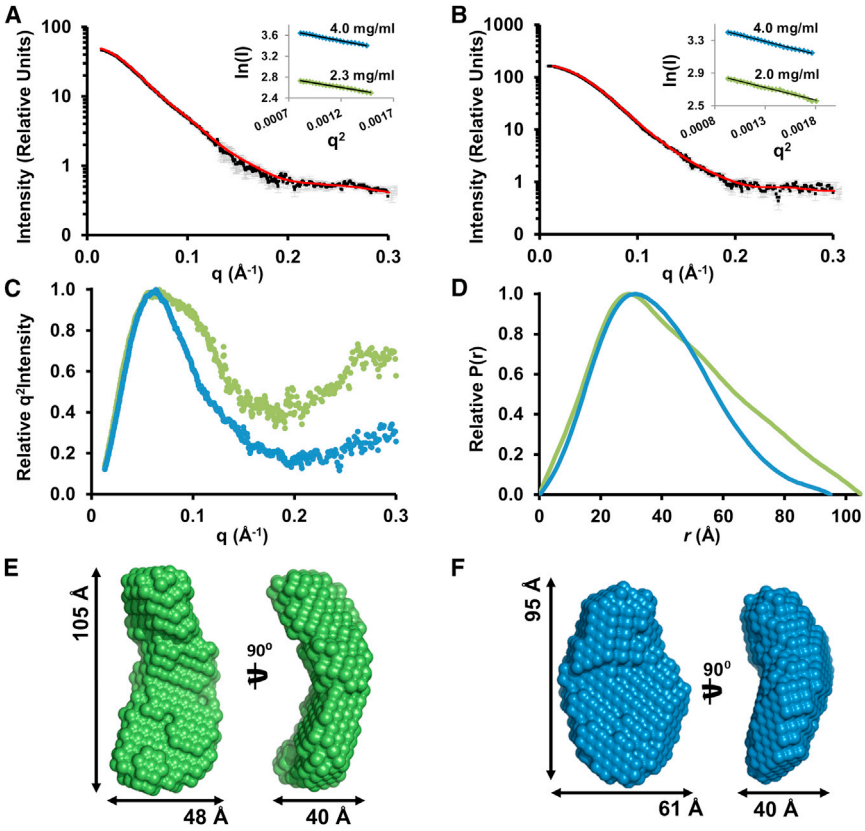

Figure 3. The p38α:PTPSL and p38α:STEP Resting-State Complex

(A) SAXS data (I(q) versus q) of the p38α:PTPSL resting-state complex shown (black squares) with error bars (gray lines). Error bars show the experimental error based on circular averaging of the 2D solution scattering data; theoretical scattering curve from ab initio molecular envelope (red); inset, Guinier plots for samples at 2.3 mg/ml and 4.0 mg/ml.

(B) SAXS data (I(q) versus q) of the p38α:STEP resting-state complex shown (black squares) with error bars (gray lines). Theoretical scattering curve from the ab initio molecular envelope (red); inset, Guinier plots for samples at 2.0 mg/ml and 4.0 mg/ml.

(C) Kratky plot of the p38α:PTPSL resting-state SAXS data (green) and p38α:STEP resting-state SAXS data (blue).

(D) P(r) function of the p38α:PTPSL resting-state complex (green) and p38α:STEP resting-state complex (blue).

(E) p38α:PTPSL ab initio molecular envelope in two views rotated by 90° with the dimensions of the envelope.

(F) The p38α:STEP ab initio molecular envelope in two views rotated by 90° with the dimensions of the envelope.

Defining the p38α Binding Site on STEP

To define the p38α binding interface on STEP, we performed reverse NMR experiments with [^{2}H,^{15}N]-STEP and unlabeled p38α. We previously published the sequence-specific backbone assignments of $STEP_{CAT}$ (Francis et al., 2013). The 2D [^{1}H,^{15}N] TROSY spectrum of STEP contains 30 additional peaks when compared to that of $STEP_{CAT,}$ in agreement with the 31 additional N-terminal residues in STEP (Figure S4D). All new peaks cluster around ~8.0 ppm, a chemical shift range typical for unstructured residues, suggesting that the KIM and KIS regions of STEP are unstructured in the unbound state, identical to what we have seen for HePTP (Figure S4D) (Francis et al., 2011a). Last, the vast majority of peaks in the STEP 2D [^{1}H,^{15}N] TROSY spectrum overlap perfectly with peaks in the $STEP_{CAT}$ 2D [^{1}H,^{15}N] TROSY spectrum, showing that the flexible N-terminal residues in STEP do not interact with $STEP_{CAT}$. This allowed for the transfer of the $STEP_{CAT}$ sequence-specific backbone assignment to STEP.

Peaks corresponding to residues 244–253, the majority of helix α0, have very different chemical shifts between STEP and $STEP_{CAT}$, indicating that the presence of the flexible N terminus (residues 214–243) alters the chemical environment of residues 244–253. This is consistent with what was observed for HePTP, in which helix α0 (residues 44–56) was also perturbed by the presence of the N terminus, residues 15–43 (Francis et al., 2011a). Previously, it was hypothesized that helix α0 must change conformation for the regulatory Ser/Thr residue at the N terminus of the helix to be phosphorylated (Mustelin et al., 2005; Szedlacsek et al., 2001). These NMR studies show that this hypothesis is correct and the pliability of helix α0 is conserved within the KIM-PTP family.

To test the effects of p38α binding on STEP, the complex between [^{2}H,^{15}N]-STEP and unlabeled p38α was purified by SEC, and a 2D [^{1}H,^{15}N] TROSY spectrum of the 78 kDa complex was immediately collected (Figure S4E). Direct comparison of the 2D [^{1}H,^{15}N] TROSY spectra of free and p38α-bound STEP reveals changes in 54 peaks, 22 of which are in fast exchange and 32 with peak line widths broadened beyond detection (Figure 4A; Figure S4E). Included in this total are 21 of the new peaks that clustered around 8.0 ppm in the free STEP spectrum that are broadened beyond detection or overlap with other peaks in the 2D [^{1}H,^{15}N] TROSY spectrum of the p38α:STEP complex. This indicates, as expected, a strong involvement of the $STEP_{KIM}$ in p38α binding. Additional new peaks unperturbed by p38α binding originate from $STEP_{KIS}$ residues that do not contribute to p38α binding. Thirty-three perturbed peaks are in $STEP_{CAT}$, including residues in helix α1′ (A263, E268, and K269), helix α2′ (F274, L276, E277, A278, E279, F280, F281, and E282), the β4–β7 loop (N376, I377, E378, E379, and M380), helix α4 (R478, T479, and F482), and helix α6 (T517, C518, Q520, and H525) (Figure 4A). Other $STEP_{CAT}$ residues that are affected include L254, A257, M285, N286, D294, T306, I307, G350, V353, and the catalytically important Q516 (Figure 4A).

3D Model of the p38α:STEP Complex

We used the NMR data, which describe the interaction interface of STEP on p38α and vice versa, together with surface accessibility data to restrain the docking of STEP and p38α using HADDOCK (the crystal structures of apo-p38α [1P38] and $STEP_{CAT}$ [2BIJ] [de Vries et al., 2007; Dominguez et al.,

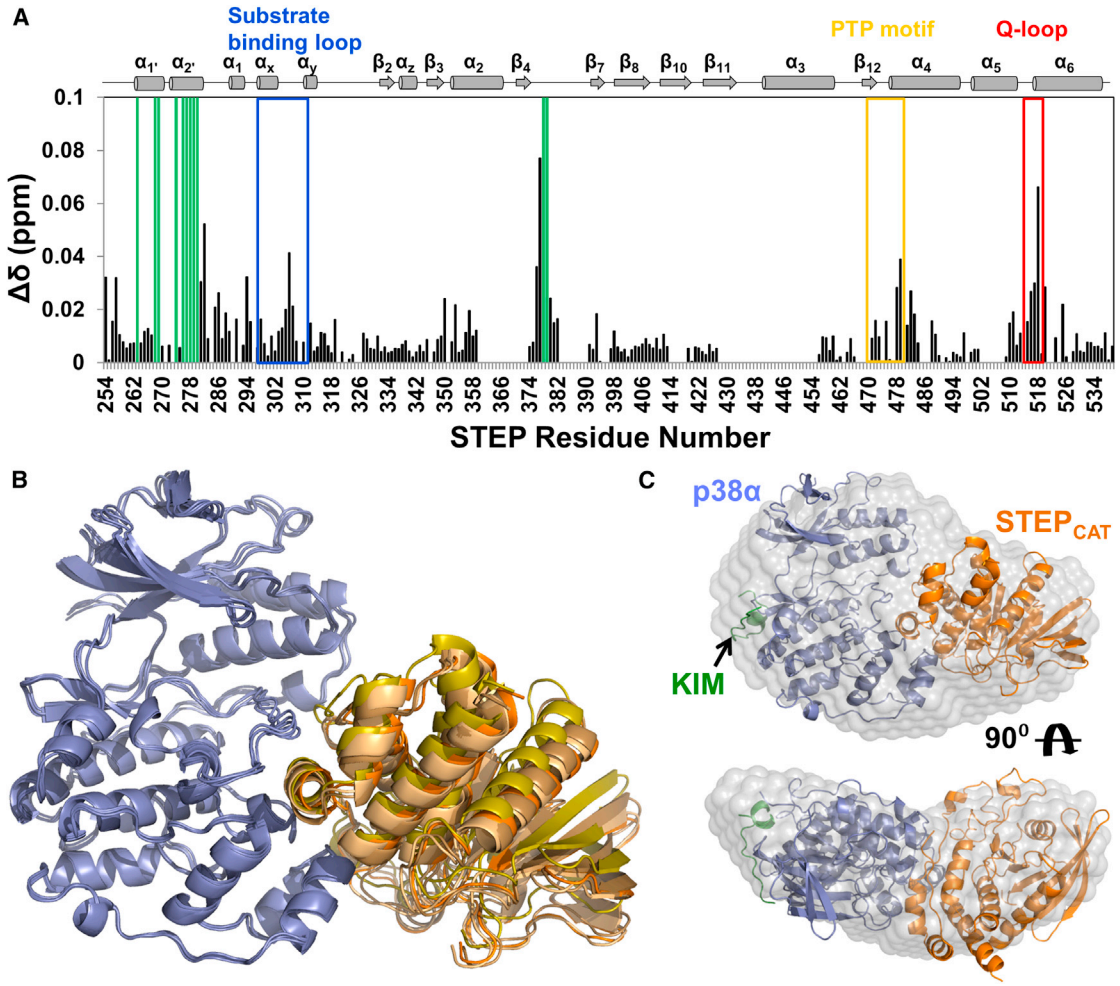

Figure 4. STEP$_{CAT}$ Binds to the p38α Activation Loop and MAPK Insert Primarily through Helix α-2′

(A) Histograms showing the combined $^1H/^{15}N$ CSP versus STEP residue for the interaction of p38α with [^2H,^{15}N]-STEP.

(B) Alignment of the four lowest energy HADDOCK structures of the p38α:STEP$_{CAT}$ complex. p38α is colored blue and STEP$_{CAT}$ is colored in shades of orange.

(C) Superposition of the lowest energy HADDOCK p38α:STEP$_{CAT}$ complex structure with the experimental SAXS molecular envelope of the p38α:STEP resting-state complex; p38α (blue), KIM (green), and STEP$_{CAT}$ (orange).

See also Figure S4.

2003; Eswaran et al., 2006; Wang et al., 1997] were used as starting structures). Although the STEP$_{CAT}$ structure does not include STEP$_{KIMKIS}$ residues (214–257), we have established—using the PSChimera—that the STEP$_{CAT}$ interaction occurred independent of a specific KIMKIS sequence. Consequently, only p38α residues affected by STEP$_{CAT}$ in both STEP and the PSChimera were used as input for the HADDOCK calculations. The lowest energy cluster produced by HADDOCK contained 76 structures with a root-mean-square deviation of 0.8 Å. The four lowest energy structures from this cluster are shown in Figure 4B. In all HADDOCK models, STEP helix α2′ binds to p38α between the activation loop and the MAPK-specific insert. The interface between the two proteins buries 2,125 ± 116 Å^2 of surface area. To experimentally test the validity of the model, we compared the calculated (determined using Hydropro; Ortega et al., 2011) R_g of the lowest energy p38α:STEP HADDOCK model (R_g = 29.2 Å) with the experimentally determined R_g (R_g = 29.9 Å). The excellent consistency of the R_gs is further supported by the excellent fit of the lowest energy p38α:STEP HADDOCK model into the molecular envelope determined for the p38α:STEP resting-state complex (NSD = 1.7; Figure 4C). Additionally, modeling the KIM peptide into the KIM binding site of p38α (based on the ERK2:HePTP$_{KIM}$ crystal structure; Zhou et al., 2006) results in, as expected, a further improved model of the p38α:STEP resting-state complex (R_g = 30.1 Å; D_{max} = 92 Å). This model, which comprises every component of the complex but the STEP$_{KIS}$, superimposes even better with the p38α:STEP molecular envelope (NSD = 1.5; Figure 4C) (Kozin and Svergun, 2001).

To further verify the model of the p38α:STEP resting-state complex, we generated a number of STEP mutants that are predicted to lead to changes in binding affinity because the mutated residues are directly involved in the p38α:STEP interaction. Indeed, mutation of residue F281 in helix α2′, and to a lesser

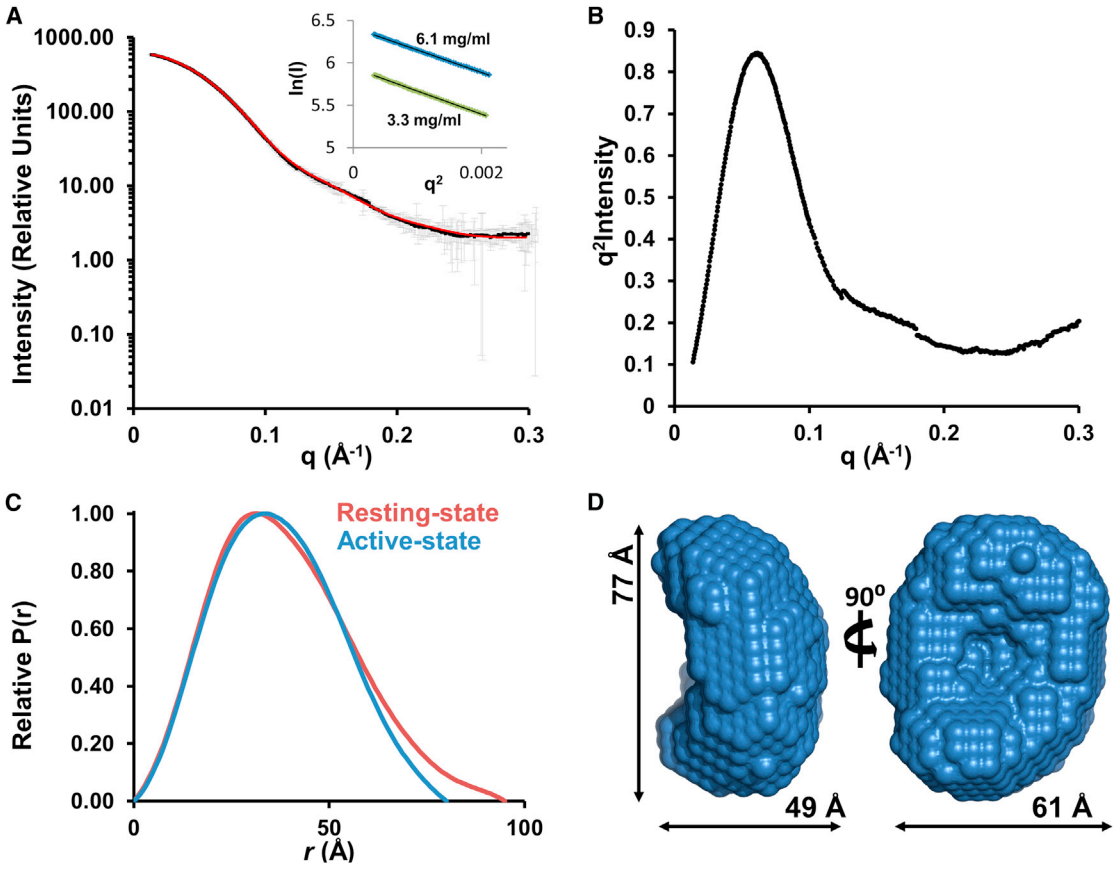

Figure 5. The p38α:STEP Active-State Complex Is More Compact Than the Resting-State Complex

(A) Experimental SAXS data (I(q) versus q) of the p38α:STEP active-state complex shown as black squares with error bars as gray lines. Error bars show the experimental error based on circular averaging of the 2D solution scattering data; theoretical scattering curve from ab initio molecular envelope (red); inset, Guinier plots for samples at 3.3 mg/ml and 6.1 mg/ml.

(B) Kratky plot.

(C) P(r) function of the p38α:STEP active-state complex (blue) overlaid with resting-state complex (red).

(D) Averaged ab initio molecular envelope; two views rotated by 90° with the dimensions of the envelope.

extent M285 and I307, showed a reduction of the binding affinity, clearly showing that helix α2′ is important for the interaction of STEP with p38α and further confirming the HADDOCK model (Table 1).

The p38α:STEP Active-State Complex

We have shown that $STEP_{CAT}$, when tethered via the KIM, interacts with p38α and perturbs residues in the p38α activation loop. However, this does not imply that STEP is poised and ready to efficiently dephosphorylate p38α. In fact, in the HADDOCK p38α:STEP resting-state complex model the STEP active site cysteine is ~35 Å away from the p38α phosphorylation loop tyrosine. Therefore, a domain arrangement must occur between the resting and active states of the p38α:STEP complex to properly position $STEP_{CAT}$ for dephosphorylation of p38α.

To verify that a domain rearrangement occurs between the active and resting states of the p38α:STEP complex, we used SAXS to determine the size and shape of the p38α:STEP active-state complex (Akella et al., 2010; Nielsen and Schwalbe, 2011). p38α was dually phosphorylated in vitro using a constitutively active mutant of MKK6. Phosphorylated p38α was incubated with a substrate-trapping mutant of STEP (C472S/T306D), the complex purified by SEC, and SAXS data recorded (Figure 5A). Using the Guinier approximation of six independent SAXS samples, an R_g of 28.5 ± 0.3 Å was calculated for the p38α:STEP active-state complex (Table 2; Figure 5A). This R_g is 1.5 Å smaller than the R_g of the resting-state complex. More striking, the D_{max} of the active-state complex, 80 Å, is 15 Å shorter than the resting-state complex (Table 2; Figures 5C and 5D). These data show that the p38α:STEP active-state complex is more compact than the resting-state complex and support that a domain rearrangement occurs between the resting and active states of the p38α:STEP complex. Thus, although $STEP_{CAT}$ interacts with p38α in the resting state, it is not properly positioned for dephosphorylation of p38α.

DISCUSSION

Our current understanding of MAPK regulation by their regulatory proteins at the molecular level is extremely limited because these essential signaling complexes have proven exceedingly difficult to investigate using traditional structural

approaches. Years of efforts to crystallize MAPK:KIM-PTP complexes have not been successful, and their large molecular weights, ~80 kDa, make NMR analysis onerous. To circumvent these problems, we examined the binding of each domain of STEP and PTPSL to p38α using NMR CSP and ITC experiments and then determined the overall molecular shape of the complexes using SAXS. Using this approach, we show that, despite having similar KIM-peptide interactions and overall binding affinities with p38α, the p38α:PTPSL and p38α:STEP resting-state complexes are surprisingly different as a result of an additional interaction of the STEP catalytic domain with p38α. These studies, in combination with complementary studies previously performed between p38α and HePTP, provide a detailed investigation of MAPK regulation by an entire family of regulators (Francis et al., 2011a).

Using NMR experiments, we show that the mode of KIM binding to p38α is conserved among the KIM-PTP family. Uniformly, $PTPSL_{KIM}$, $STEP_{KIM}$, and $HePTP_{KIM}$ engaged residues within the three hydrophobic pockets and perturbed residues at the CD site. In contrast, crystal structures of p38α bound to KIM peptides of the activating kinases, MKK3b and MKK6, reveal a different mode of binding in which only hydrophobic pockets Φ_A and Φ_B are engaged and an extensive electrostatic interaction with the CD site is absent (Chang et al., 2002; Garai et al., 2012). This demonstrates a critical point in MAPK selectivity; the mechanism of KIM binding to p38α is different for each class of regulators (i.e., MAPKKs versus KIM-PTPs).

Based on NMR and SAXS data, the interaction of resting-state p38α with PTPSL is similar to that described previously between p38α and HePTP. However, the p38α:PTPSL and p38α:HePTP interactions are not identical. One key feature of the p38α:HePTP interaction, the extensive interaction between p38α and the $HePTP_{KIS}$, is not observed between p38α and the $PTPSL_{KIS}$ (Francis et al., 2011a). Despite the limited interaction surface between p38α and PTPSL, PTPSL binds p38α nearly six times tighter than HePTP does. Recently published in vitro phosphatase assays showed that although HePTP and PTPSL can both readily dephosphorylate p38α, PTPSL is the most efficient p38α phosphatase of all tested (Zhang et al., 2011). This is likely the product of (1) the highest affinity interaction with p38α among the KIM-PTPs and (2) the limited interaction outside of the KIM, imposing minimal constraints on the flexibility and movement of the $PTPSL_{CAT}$.

In contrast, the p38α:STEP resting-state complex is more compact than the other two p38α:KIM-PTP resting-state complexes because of an additional previously unidentified interaction between $STEP_{CAT}$ and p38α. In the resting-state complex, $STEP_{CAT}$ occludes a pocket on p38α formed between the MAPK insert and the C lobe that has been shown to bind allosteric signaling molecules that are known activators of the p38α cascade, such as fatty acids (Diskin et al., 2008; Nony et al., 2005; Perry et al., 2009). Binding of certain lipid-based molecules to this pocket has been shown to promote autophosphorylation and activation of p38α in vitro (Gills et al., 2007; Tzarum et al., 2012). STEP regulates p38α at the site of extrasynaptic glutamate receptors, where overactivation of the kinase leads to the production of proapoptotic signals culminating in neuronal cell death (Poddar et al., 2010). Therefore, STEP may have adapted several means to suppress p38α activity in the resting state. First, by binding strongly to the KIM binding site, STEP prevents upstream activating kinases from promiscuously binding and activating p38α. Second, by blocking access to the MAPK insert pocket, through the $STEP_{CAT}$ interaction, STEP can prevent the binding of allosteric signaling molecules that induce autoactivation of p38α.

The orientation of $STEP_{CAT}$ in the p38α:STEP resting-state complex is not conducive to dephosphorylation of the tyrosine residue in the p38α phosphorylation loop and significant rotation of $STEP_{CAT}$ is necessary to properly position the active site for catalysis. This domain rearrangement is evident when comparing SAXS data of the resting and active states of the p38α:STEP complex. A study conducted by Zhang et al. showed that STEP is significantly less efficient than PTPSL and HePTP at dephosphorylating p38α. The k_{cat} for the STEP-catalyzed dephosphorylation of p38α is ~20-fold lower than those for PTPSL or HePTP, showing that it is likely easier to move the flexibly tethered $HePTP_{CAT}$ and $PTPSL_{CAT}$ than moving the "trapped" (i.e., p38α-bound) $STEP_{CAT}$ (Balasu et al., 2009; Zhang et al., 2011).

Taken together, these results provide fundamental insights into the molecular basis of p38α regulation by the neuronal KIM-PTPs. We have identified how STEP prevents promiscuous activation of p38α by blocking access to the MAPK insert pocket. Because p38α has been implicated in the pathogenesis of numerous neurological disorders, these findings could facilitate the development of new drug therapies to treat these disorders.

EXPERIMENTAL PROCEDURES

Peptide and Protein Preparation

The $PTPSL_{KIM}$ peptide (IGLQERRGSNVSLTLDM), $STEP_{KIM}$ (MGLQERR GSNVSLTLDM), and $STEP_{KIMKIS}$ (MGLQERRGSNVSLTLDMCTPGCNEEGFG YLVSPREESAHEYLLS) were synthesized, HPLC purified, and verified by mass spectrometry (MS) (>98% purity; Biosynthesis).

Expression and purification of unphosphorylated p38α was carried out as previously described (Francis et al., 2011a). PTPSL (residues 332–655), $PTPSL_{CAT}$ (residues 361–655), STEP (residues 214–539), $STEP_{CAT}$ (residues 244–539), and PSChimera (PTPSL residues 332–373 with STEP residues 257–539; gene synthesized by DNA 2.0) were expressed and purified using the protocol previously described in detail for $STEP_{CAT}$ (Francis et al., 2013). STEP (residues 214–539) mutants F274A/F281A, F280A/I307A, and M285A/I307A were produced by quick-change mutagenesis.

The $PTPSL_{KIMKIS}$ (residues 332–373) was subcloned into a derivative of the pET28 vector that includes an N-terminal His_6-tag and a TEV protease recognition sequence (Peti and Page, 2007). The expression vector was transformed into BL21-(DE3) RIL *E. coli* cells (Invitrogen). Cultures were grown in Luria broth at 37°C with shaking at 250 rpm until reaching an optical density (OD_{600}) between 0.6 and 0.8, at which point expression was induced by the addition of 1.0 mM isopropylthio-β-D-galactoside (IPTG, final concentration). The cultures were grown for an additional 3 hr at 37°C with shaking at 250 rpm. The cells were harvested by centrifugation (6,000 × *g*, 12 min, 4°C) and stored at −80°C until purification. All buffers and glassware used for purification were autoclaved prior to purification. For purification, cell pellets were resuspended in lysis buffer (50 mM Tris [pH 8.0], 500 mM NaCl, 5 mM imidazole, 0.1% Triton X-1000, and cOmplete EDTA-free protease inhibitor cocktail tablets; Roche) and lysed by high-pressure homogenization (Avestin C3 Emulsiflex). The bacterial lysate was cleared by centrifugation (35,000 × *g*, 40 min, 4°C). After filtration, the supernatant was loaded onto a 5 ml HisTrap HP column (GE Healthcare) equilibrated with Buffer A (50 mM Tris [pH 8.0], 500 mM NaCl, and 5 mM imidazole). Protein was eluted from the column using a 5–500 mM imidazole gradient over 20 column

volumes. Purified fractions were pooled, and the His_6-tag was removed by incubation with TEV protease during overnight dialysis in 50 mM Tris (pH 8.0), 500 mM NaCl at 4°C. The TEV protease, the His_6-tag, and uncleaved protein were removed using a second IMAC step. Final purification was achieved using size exclusion chromatography (SEC) equilibrated in 50 mM Tris (pH 6.8), 500 mM NaCl. The molecular weight of the purified peptide was verified by electrospray-ionization MS.

All unlabeled, purified proteins were stored at −80°C until use, at which point they were thawed and equilibrated in the appropriate buffer using SEC. All labeled proteins for NMR analysis were purified within 24 hr of data acquisition and stored on ice. $PTPSL_{KIM}$, $STEP_{KIM}$, and $STEP_{KIMKIS}$ peptides were solubilized in the appropriate buffer prior to the experiment. The final protein buffer was dependent on the experiment performed. For ITC experiments, the final SEC purification was performed in ITC buffer (10 mM Tris pH 7.5, 150 mM NaCl, 0.1 mM EDTA, 0.5 mM TCEP); for NMR and SAXS experiments, the final SEC purification was performed in NMR buffer (50 mM HEPES [pH 6.8], 150 mM NaCl, 5 mM dithiothreitol).

NMR Sample Preparation

[^{2}H,^{15}N]-p38α (Vogtherr et al., 2005) and [^{2}H,^{15}N]-STEP were expressed in M9 media supplemented with $^{15}NH_4Cl$ (1 g/l) in 99% D_2O and purified as previously described. $PTPSL_{KIM}$, $PTPSL_{KIMKIS}$, $STEP_{KIM}$, or $STEP_{KIMKIS}$ peptides were added to [^{2}H,^{15}N]-p38α (100 μM p38α) in the following molar excesses: $PTPSL_{KIM}$ (1:1 and 1:8 molar ratios, p38:peptide), $PTPSL_{KIMKIS}$ (1:1 and 1:3 molar ratios, p38:peptide), $STEP_{KIM}$ (1:1, 1:3, 1:5, and 1:8 molar ratios, p38:peptide), and $STEP_{KIMKIS}$ (1:1, 1:3, 1:6, and 1:8 molar ratios, p38:peptide). $PTPSL_{CAT}$ and $STEP_{CAT}$ were added to [^{2}H,^{15}N]-p38α (100 μM p38α) in a twofold molar excess (0.1 mM [^{2}H,^{15}N]-p38α:0.2 mM $PTPSL_{CAT}$ or $STEP_{CAT}$). For p38α:KIM-PTP complex formation, [^{2}H,^{15}N]-p38α was incubated with either PTPSL, STEP, or PSChimera (1:1 molar ratio) on ice for 45 min and purified using SEC (Superdex 75 26/60, NMR buffer). Each p38α:KIM-PTP complex elutes at the position expected for the p38α:KIM-PTP heterodimer. Each [^{2}H,^{15}N]-p38α:KIM-PTP complex was concentrated to 0.1 mM and stored on ice (<8 hr) until NMR data acquisition. For the p38α:[^{2}H,^{15}N]-STEP complex formation, [^{2}H,^{15}N]-STEP was incubated with p38α (1:1 molar ratio) on ice for 45 min and purified using SEC (Superdex 75 26/60, NMR buffer). The p38α:[^{2}H,^{15}N]-STEP complex was concentrated to 0.1 mM and stored on ice (<2 hr) until NMR data acquisition. A 2D [^{1}H,^{15}N]-TROSY spectrum was recorded for all samples described above. All NMR experiments were performed at 298 K on a Bruker Advance 800 MHz spectrometer equipped with a TCI HCN z-gradient cryoprobe. NMR samples were prepared in NMR buffer in 90% H_2O/10% D_2O. The NMR spectra were processed with Topspin 2.1/3.0/3.1 (Bruker) and analyzed using CARA (http://cara.nmr.ch).

Chemical Shift Perturbation Studies

The p38α:$STEP_{KIM}$ and p38α: $PTPSL_{KIM}$ peptide titration series (1:1, 1:3, 1:5, and 1:8 ratios, p38α:$STEP_{KIM}$) were used to follow chemical shift changes in p38α upon peptide or protein binding. Nearly all peaks showed fast exchange and thus could be easily tracked. The observed trajectory of each peak was applied to the analysis of the KIMKIS peptides ($PTPSL_{KIMKIS}$ and $STEP_{KIMKIS}$) and the full-length complexes (PTPSL, STEP, and PSChimera), allowing for high certainty of peak assignments of p38α in the bound conformations. All chemical shift differences (Δδ) were calculated using

$$\Delta\delta(ppm) = \sqrt{(\Delta\delta_H)^2 + \left(\frac{\Delta\delta_N}{10}\right)^2}.$$

To allow for direct comparison across all CSP experiments, we used identical cut-off CSPs as in the HePTP NMR experiments; small CSP 0.07–0.103 ppm, medium CSP 0.104–0.131 ppm, and large CSP ≥0.132 (Francis et al., 2011a).

HADDOCK Calculations

HADDOCK was used to dock p38α and STEP using ambiguous NMR-derived restraints. p38α (PBDID 1P38) and STEP (PBDID 2BIJ) were used as starting input. Active residues were defined as those that undergo a CSP and have high solvent accessibility in the unbound protein structure (p38α residues: 177, 179, 183, 222, 248, 254, and 256; STEP residues: 263, 268, 269, 274, 277, 278, 279, 281, 282, 285, 286, 294, 306, 307, 377, 378, 379, 516, 517, and 518). Passive residues have a CSP but low solvent accessibility (p38α residues: 190, 195, 247, 255, and 328; STEP residues: 276, 280, 350, 353, 376, 380, 478, 479, 482, 520, and 525). CSPs were the only experimental restraint type used in the HADDOCK calculation and default settings were used for all docking steps, as used by the easy interface of the HADDOCK web server (http://haddock.science.uu.nl/enmr/services/HADDOCK).

Isothermal Titration Calorimetry

ITC experiments were performed at 25°C using a VP-ITC microcalorimeter (Microcal). Titrant (10 μl per injection) was injected into the sample cell over a period of 20 s with a 250 s interval between titrations to allow for complete equilibration and baseline recovery. Twenty-eight injections were delivered during each experiment, and the solution in the sample cell was stirred at 307 rpm to ensure rapid mixing. To determine the thermodynamic parameters (Δ*H*, Δ*S*, and Δ*G*) and binding constants (*K*) of the p38α:$PTPSL_{KIM}$, p38α:PTPSL, and p38α:STEP interactions, $PTPSL_{KIM}$, PTPSL, and STEP were titrated into the p38α. To determine the same parameters for the p38α:$STEP_{KIM}$, p38α:$PTPSL_{KIMKIS}$, p38α:$STEP_{KIMKIS}$, and p38α:PSChimera interaction, p38α was titrated into the protein. For all titrations the concentrations were slightly varied to ensure independence of the K_d from the protein/peptide concentrations. Data were analyzed with a one-site binding model assuming a binding stoichiometry of 1:1 using Origin 7.0 software. A nonlinear least-squares algorithm and the titrant and sample cell concentrations were used to fit the heat flow per injection to an equilibrium binding equation, providing values of the stoichiometry (*n*), change in enthalpy (Δ*H*), and binding constant (*K*). All data were repeated in triplicate.

Small-Angle X-Ray Scattering

For the resting-state p38α: PTPSL and p38α:STEP complexes, purified, unphosphorylated p38α was incubated in a 1:1 molar ratio with purified $PTPSL_{331–655}$ and/or purified $STEP_{214–539}$ on ice for 30 min and the complexes purified using SEC (Superdex 75 26/60, NMR buffer). To form the active-state complex of p38α:STEP, purified, dually phosphorylated p38α was incubated in a 1:1 molar ratio with purified $STEP_{214–539}$ T306D/C472S on ice for 30 min and the complex was purified using SEC (Superdex 75 26/60, NMR buffer). For p38α:PTPSL, data were collected on samples at 0.4, 0.8, 1.6, 2.3, and 4.0 mg/ml. For resting-state p38α:STEP, data were collected on samples at 1.0, 2.0, and 4.0 mg/ml. For active-state p38α:STEP, data were collected on samples at 0.8, 3.3, and 6.1 mg/ml. All samples were prepared within 48 hr of data acquisition and stored on ice at 4°C. All samples were filtered (0.02 μM filter, Whatman) immediately prior to data collection. All data were recorded at beamline X9 at the National Synchrotron Light Source (NSLS) using a Dectris pilatus 300k (p38α:PTPSL and active-state p38α:STEP; 3.4 m distance from the sample for SAXS) or a MarCCD 165 (resting-state p38α:STEP; 3.4 m distance from the sample for SAXS) and a Photonic Science CCD (0.47 m from the sample for WAXS) detector. Twenty microliters of sample was continuously flowed through a 1 mm diameter capillary and exposed to an X-ray beam for 30 s (p38α:PTPSL), 60 s (active-state p38α:STEP), or 180 s (resting-state p38α:STEP). Normalization for beam intensity, buffer subtraction, and merging of the data from both detectors was carried out using PRIMUS (Konarev et al., 2003). A Guinier approximation, $I(q) = I(0)\exp(-q^2R_g^2 / 3)$, where a plot of $\ln[I(q)]$ and q^2 is linear for $q < 1.3/R_g$, was performed on at least four independent scattering trials and averaged to determine the radius of gyration. The linearity of the Guinier region and the intensity at zero scattering angle, I(0), were used to validate that all samples were monodisperse in solution. I(0)/c, where c is concentration, was consistent for all measurements for a single complex. GNOM (Svergun, 1992) was used to determine the pair-distribution function, P(r), for each complex. Twenty-four envelopes were generated for each complex using GASBOR (Svergun et al., 2001) and were aligned and averaged using the DAMAVER program suite (Volkov and Svergun, 2003).

SUPPLEMENTAL INFORMATION

Supplemental Information includes Supplemental Experimental Procedures and four figures and can be found with this article online at http://dx.doi.org/10.1016/j.str.2013.07.003.

ACKNOWLEDGMENTS

The authors thank Drs. L. Yang and M. Allaire (NSLS) for their support at NSLS beamline. We thank Dr. Paul Lombroso, Yale University, for providing PTPN5 DNA. This research was supported by grant RSG-08-067-01-LIB from the American Cancer Society to R.P. and by R01GM100910 from the National Institutes of Health to W.P. Use of NSLS at Brookhaven National Laboratory was supported by the U.S. Department of Energy, Office of Science, Office of Basic Energy Sciences under contract no. DE-AC02-98CH10886. Eight hundred megahertz NMR data were recorded at Brandeis University; the instrument was purchased with support from NIH S10-RR017269.

Received: March 12, 2013
Revised: June 24, 2013
Accepted: July 2, 2013
Published: August 8, 2013

REFERENCES

Akella, R., Min, X., Wu, Q., Gardner, K.H., and Goldsmith, E.J. (2010). The third conformation of p38α MAP kinase observed in phosphorylated p38α and in solution. Structure *18*, 1571–1578.

Balasu, M.C., Spiridon, L.N., Miron, S., Craescu, C.T., Scheidig, A.J., Petrescu, A.J., and Szedlacsek, S.E. (2009). Interface analysis of the complex between ERK2 and PTP-SL. PLoS ONE *4*, e5432.

Blanco-Aparicio, C., Torres, J., and Pulido, R. (1999). A novel regulatory mechanism of MAP kinases activation and nuclear translocation mediated by PKA and the PTP-SL tyrosine phosphatase. J. Cell Biol. *147*, 1129–1136.

Chang, C.I., Xu, B.E., Akella, R., Cobb, M.H., and Goldsmith, E.J. (2002). Crystal structures of MAP kinase p38 complexed to the docking sites on its nuclear substrate MEF2A and activator MKK3b. Mol. Cell *9*, 1241–1249.

Chirivi, R.G., Dilaver, G., van de Vorstenbosch, R., Wanschers, B., Schepens, J., Croes, H., Fransen, J., and Hendriks, W. (2004). Characterization of multiple transcripts and isoforms derived from the mouse protein tyrosine phosphatase gene *Ptprr*. Genes Cells *9*, 919–933.

de Vries, S.J., van Dijk, A.D., Krzeminski, M., van Dijk, M., Thureau, A., Hsu, V., Wassenaar, T., and Bonvin, A.M. (2007). HADDOCK versus HADDOCK: new features and performance of HADDOCK2.0 on the CAPRI targets. Proteins *69*, 726–733.

Dérijard, B., Raingeaud, J., Barrett, T., Wu, I.H., Han, J., Ulevitch, R.J., and Davis, R.J. (1995). Independent human MAP-kinase signal transduction pathways defined by MEK and MKK isoforms. Science *267*, 682–685.

Diskin, R., Engelberg, D., and Livnah, O. (2008). A novel lipid binding site formed by the MAP kinase insert in p38 alpha. J. Mol. Biol. *375*, 70–79.

Dominguez, C., Boelens, R., and Bonvin, A.M. (2003). HADDOCK: a protein-protein docking approach based on biochemical or biophysical information. J. Am. Chem. Soc. *125*, 1731–1737.

Eswaran, J., von Kries, J.P., Marsden, B., Longman, E., Debreczeni, J.E., Ugochukwu, E., Turnbull, A., Lee, W.H., Knapp, S., and Barr, A.J. (2006). Crystal structures and inhibitor identification for PTPN5, PTPRR and PTPN7: a family of human MAPK-specific protein tyrosine phosphatases. Biochem. J. *395*, 483–491.

Francis, D.M., Różycki, B., Koveal, D., Hummer, G., Page, R., and Peti, W. (2011a). Structural basis of p38α regulation by hematopoietic tyrosine phosphatase. Nat. Chem. Biol. *7*, 916–924.

Francis, D.M., Różycki, B., Tortajada, A., Hummer, G., Peti, W., and Page, R. (2011b). Resting and active states of the ERK2:HePTP complex. J. Am. Chem. Soc. *133*, 17138–17141.

Francis, D.M., Page, R., and Peti, W. (2013). Sequence-specific backbone (1)H, (13)C and (15)N assignments of the 34 kDa catalytic domain of PTPN5 (STEP). Biomol. NMR Assign.

Garai, A., Zeke, A., Gógl, G., Törő, I., Fördős, F., Blankenburg, H., Bárkai, T., Varga, J., Alexa, A., Emig, D., et al. (2012). Specificity of linear motifs that bind to a common mitogen-activated protein kinase docking groove. Sci. Signal. *5*, ra74.

Gills, J.J., Castillo, S.S., Zhang, C., Petukhov, P.A., Memmott, R.M., Hollingshead, M., Warfel, N., Han, J., Kozikowski, A.P., and Dennis, P.A. (2007). Phosphatidylinositol ether lipid analogues that inhibit AKT also independently activate the stress kinase, p38alpha, through MKK3/6-independent and -dependent mechanisms. J. Biol. Chem. *282*, 27020–27029.

Hendriks, W., Schepens, J., Brugman, C., Zeeuwen, P., and Wieringa, B. (1995). A novel receptor-type protein tyrosine phosphatase with a single catalytic domain is specifically expressed in mouse brain. Biochem. J. *305*, 499–504.

Kim, E.K., and Choi, E.J. (2010). Pathological roles of MAPK signaling pathways in human diseases. Biochim. Biophys. Acta *1802*, 396–405.

Konarev, P.V., Volkov, V.V., Sokolova, A.V., Koch, M.H.J., and Svergun, D.I. (2003). PRIMUS: a Windows PC-based system for small-angle scattering data analysis. J. Appl. Cryst. *36*, 1277–1282.

Kozin, M.B., and Svergun, D.I. (2001). Automated matching of high- and low-resolution structural models. J. Appl. Cryst. *34*, 33–41.

Larkin, M.A., Blackshields, G., Brown, N.P., Chenna, R., McGettigan, P.A., McWilliam, H., Valentin, F., Wallace, I.M., Wilm, A., Lopez, R., et al. (2007). Clustal W and Clustal X version 2.0. Bioinformatics *23*, 2947–2948.

Lombroso, P.J., Murdoch, G., and Lerner, M. (1991). Molecular characterization of a protein-tyrosine-phosphatase enriched in striatum. Proc. Natl. Acad. Sci. USA *88*, 7242–7246.

Lombroso, P.J., Naegele, J.R., Sharma, E., and Lerner, M. (1993). A protein tyrosine phosphatase expressed within dopaminoceptive neurons of the basal ganglia and related structures. J. Neurosci. *13*, 3064–3074.

Muñoz, J.J., Tárrega, C., Blanco-Aparicio, C., and Pulido, R. (2003). Differential interaction of the tyrosine phosphatases PTP-SL, STEP and HePTP with the mitogen-activated protein kinases ERK1/2 and p38alpha is determined by a kinase specificity sequence and influenced by reducing agents. Biochem. J. *372*, 193–201.

Mustelin, T., Tautz, L., and Page, R. (2005). Structure of the hematopoietic tyrosine phosphatase (HePTP) catalytic domain: structure of a KIM phosphatase with phosphate bound at the active site. J. Mol. Biol. *354*, 150–163.

Nielsen, G., and Schwalbe, H. (2011). NMR spectroscopic investigations of the activated p38α mitogen-activated protein kinase. ChemBioChem *12*, 2599–2607.

Nony, P.A., Kennett, S.B., Glasgow, W.C., Olden, K., and Roberts, J.D. (2005). 15S-Lipoxygenase-2 mediates arachidonic acid-stimulated adhesion of human breast carcinoma cells through the activation of TAK1, MKK6, and p38 MAPK. J. Biol. Chem. *280*, 31413–31419.

Ortega, A., Amorós, D., and García de la Torre, J. (2011). Prediction of hydrodynamic and other solution properties of rigid proteins from atomic- and residue-level models. Biophys. J. *101*, 892–898.

Perry, J.J., Harris, R.M., Moiani, D., Olson, A.J., and Tainer, J.A. (2009). p38alpha MAP kinase C-terminal domain binding pocket characterized by crystallographic and computational analyses. J. Mol. Biol. *391*, 1–11.

Peti, W., and Page, R. (2007). Strategies to maximize heterologous protein expression in *Escherichia coli* with minimal cost. Protein Expr. Purif. *51*, 1–10.

Piserchio, A., Francis, D.M., Koveal, D., Dalby, K.N., Page, R., Peti, W., and Ghose, R. (2012). Docking interactions of hematopoietic tyrosine phosphatase with MAP kinases ERK2 and p38α. Biochemistry *51*, 8047–8049.

Poddar, R., Deb, I., Mukherjee, S., and Paul, S. (2010). NR2B-NMDA receptor mediated modulation of the tyrosine phosphatase STEP regulates glutamate induced neuronal cell death. J. Neurochem. *115*, 1350–1362.

Saxena, M., Williams, S., Taskén, K., and Mustelin, T. (1999). Crosstalk between cAMP-dependent kinase and MAP kinase through a protein tyrosine phosphatase. Nat. Cell Biol. *1*, 305–311.

Svergun, D. (1992). Determination of the regularization parameter in indirect-transform methods using perceptual criteria. J. Appl. Cryst. *25*, 495–503.

Svergun, D.I., Petoukhov, M.V., and Koch, M.H. (2001). Determination of domain structure of proteins from X-ray solution scattering. Biophys. J. *80*, 2946–2953.

Szedlacsek, S.E., Aricescu, A.R., Fulga, T.A., Renault, L., and Scheidig, A.J. (2001). Crystal structure of PTP-SL/PTPBR7 catalytic domain: implications for MAP kinase regulation. J. Mol. Biol. *311*, 557–568.

Tárrega, C., Blanco-Aparicio, C., Muñoz, J.J., and Pulido, R. (2002). Two clusters of residues at the docking groove of mitogen-activated protein kinases differentially mediate their functional interaction with the tyrosine phosphatases PTP-SL and STEP. J. Biol. Chem. *277*, 2629–2636.

Tzarum, N., Eisenberg-Domovich, Y., Gills, J.J., Dennis, P.A., and Livnah, O. (2012). Lipid molecules induce p38α activation via a novel molecular switch. J. Mol. Biol. *424*, 339–353.

Van Den Maagdenberg, A.M., Bächner, D., Schepens, J.T., Peters, W., Fransen, J.A., Wieringa, B., and Hendriks, W.J. (1999). The mouse *Ptprr* gene encodes two protein tyrosine phosphatases, PTP-SL and PTPBR7, that display distinct patterns of expression during neural development. Eur. J. Neurosci. *11*, 3832–3844.

Vogtherr, M., Saxena, K., Grimme, S., Betz, M., Schieborr, U., Pescatore, B., Langer, T., and Schwalbe, H. (2005). NMR backbone assignment of the mitogen-activated protein (MAP) kinase p38. J. Biomol. NMR *32*, 175.

Volkov, V.V., and Svergun, D.I. (2003). Uniqueness of *ab initio* shape determination in small-angle scattering. J. Appl. Cryst. *36*, 860–864.

Wang, Z., Harkins, P.C., Ulevitch, R.J., Han, J., Cobb, M.H., and Goldsmith, E.J. (1997). The structure of mitogen-activated protein kinase p38 at 2.1-A resolution. Proc. Natl. Acad. Sci. USA *94*, 2327–2332.

Xu, J., Kurup, P., Zhang, Y., Goebel-Goody, S.M., Wu, P.H., Hawasli, A.H., Baum, M.L., Bibb, J.A., and Lombroso, P.J. (2009). Extrasynaptic NMDA receptors couple preferentially to excitotoxicity via calpain-mediated cleavage of STEP. J. Neurosci. *29*, 9330–9343.

Zanke, B., Suzuki, H., Kishihara, K., Mizzen, L., Minden, M., Pawson, A., and Mak, T.W. (1992). Cloning and expression of an inducible lymphoid-specific, protein tyrosine phosphatase (HePTPase). Eur. J. Immunol. *22*, 235–239.

Zhang, Y.Y., Wu, J.W., and Wang, Z.X. (2011). Mitogen-activated protein kinase (MAPK) phosphatase 3-mediated cross-talk between MAPKs ERK2 and p38alpha. J. Biol. Chem. *286*, 16150–16162.

Zhou, T., Sun, L., Humphreys, J., and Goldsmith, E.J. (2006). Docking interactions induce exposure of activation loop in the MAP kinase ERK2. Structure *14*, 1011–1019.